



Switchback Patches Evolve into Microstreams via Magnetic Relaxation

Shirsh Lata Soni¹ , Mojtaba Akhavan-Tafti¹ , Gabriel Ho Hin Suen² , Justin Kasper¹ , Marco Velli³ ,
Rossana De Marco⁴ , Liang Zhao¹ , and Christopher J Owen²

¹ Department of Climate and Space Science, University of Michigan, MI, USA; 155365966@qq.com

² Mullard Space Science Laboratory, University College London, UK

³ Department of Earth, Planetary and Space Sciences, University of California, Los Angeles, CA, USA

⁴ National Institute for Astrophysics, Institute for Space Astrophysics and Planetology, Roma, Italy

Received 2024 February 13; revised 2024 November 05; accepted 2024 November 17; published 2024 December 19

Abstract

Switchbacks, defined as Alfvénic reversals in magnetic field polarity, can dissipate their magnetic energy with heliocentric distance. To further investigate this, two distinct solar wind parcels tracing back to a similar solar source region were examined during a radial alignment between Parker Solar Probe (@25.8RS) and Solar Orbiter (@152RS). The one caveat was that the two probes were located on opposite sides of the heliospheric current sheet during the alignment. The two parcels contained a multitude of switchbacks—the parcel closer to the Sun was characterized as a switchback patch (SBP), where background proton velocity (v_p) is comparable to the pristine solar wind (v_{sw}), while the parcel farther from the Sun showed characteristics attributable to a microstream (MS; $v_p > v_{sw}$). It was found that (1) MS contains, on average, 30% fewer switchbacks than SBP, and (2) dynamic and thermal pressures decreased by up to 20% across switchback boundaries in SBP and relatively unchanged in MS. Magnetic relaxation can explain the lower number of switchbacks in MS compared to SBP. Switchback relaxation inside SBP can, in turn, accelerate plasma inside SBP over time and heliocentric distance, thus resulting in $v_p > v_{sw}$ in MS. Therefore, it is hypothesized that magnetic relaxation of switchbacks may cause SBPs to evolve into MSs over time and heliocentric distance.

Unified Astronomy Thesaurus concepts: [The Sun \(1693\)](#); [Solar wind \(1534\)](#); [Solar magnetic reconnection \(1504\)](#)

1. Introduction

The origin and evolution of switchbacks—intense, localized rotations in the magnetic field—remain key open questions in heliospheric physics (M. Neugebauer et al. 1995; S. W. Kahler et al. 1996, F. S. Mozer et al. 2020). These large amplitude Alfvénic fluctuations were first observed near the Sun but linked to ubiquitous turbulence farther out in the heliosphere. Unraveling this connection requires tracking switchbacks over radial distances. During the 3 yr span following the launch of the Parker Solar Probe (hereafter PSP) and the Solar Orbiter (hereafter SolO) missions, favorable orbital configurations have facilitated multi-point observations. These observations will provide insights into the evolution of switchbacks in relation to heliocentric distance and the solar wind conditions influenced by their progression. PSP’s close-approach observations have revealed switchbacks to be ubiquitous near the Sun, occurring in both slow and fast wind streams (S. D. Bale et al. 2019; J. C. Kasper et al. 2019). Meanwhile, SolO has also detected switchback-like structures from its vantage point farther from the Sun (A. Fedrova et al. 2021).

Switchbacks are discrete, impulsive, antisunward propagating Alfvénic fluctuations. Near the Sun, the amplitude of the magnetic field deflection can be larger than the field magnitude and, hence, the radial component of the magnetic field (B_r) can fully reverse, leading to bulk speed enhancements of up to twice the local Alfvén speed, v_A . Therefore, switchbacks carry significant momentum and kinetic energy and appear to be an important aspect of solar wind dynamics. Switchbacks are short on timescales of seconds to minutes, they also generally occur in

patches—dense adjacent B_r reversals lasting for several minutes to hours that are separated by quieter regions of near-radial magnetic field. On the other hand, microstreams (MSs) are fluctuations in the solar wind speed and density associated with polarity-reversing folds in the radial component of the magnetic field that last for minutes to hours (M. Neugebauer et al. 1995; M. Neugebauer and A. C. Sterling, 2021). A natural question arises here: are these magnetic structures of solar wind associated with each other?

Various mechanisms have been proposed to explain the development of switchbacks. They are hypothesized to result from processes within the corona, such as interchange reconnection (J. F. Drake et al. 2021; G. P. Zank et al. 2020). Additionally, in a high beta plasma environment, they could stem from instabilities like the firehose (A. Tenerani and M. Velli, 2018), which often leads to the formation of highly kinked field lines. Furthermore, switchbacks may dynamically form as turbulent fluctuations propagate into the inner heliosphere, induced by shear flows or the expansion of the solar wind itself (S. Landi et al. 2006; D. Ruffolo et al. 2020; J. Squire et al. 2020; A. Mallet et al. 2021; N. A. Schwadron and D. J. McComas, 2021). A. Tenerani et al. (2021a), suggested that the switchbacks can be generated by the expansion of the solar wind, and additionally found that the occurrence of switchbacks in the solar wind evolves in a scale-dependent manner: the proportion of longer-duration switchbacks increases with radial distance, while it decreases for shorter switchbacks. This suggests that switchback dynamics involve a complex interplay of decay and in situ generation in the inner heliosphere.

Studies have shown (A. A. van Ballegooijen et al. 2011, V. Montagud-Camps et al. 2018, M. Akhavan-Tafti and S. L. Soni 2024) that the radial expansion of the solar wind plays an important role in the formation of switchbacks. Small amplitude waves propagating outwards from the Sun evolve

Table 1
Radial Alignment Durations of PSP and SoLO, Their Distance from Sun

SN	Alignment Duration	PSP (Rs)	Solo (Rs)
1	2020-09-26T20:30:00-2020-09-27T07:30:00	25.8 (Enc. 6)	210
2.	2021-04-28T20:30:00-2021-04-29T04:30:00	17 (Enc. 8)	191
3.	2021-08-11T08:30:00-2021-08-12T09:30:00	25.8 (Enc.9)	152
4.	2021-09-13T11:30:00-2021-09-24T08:30:00	157	126.8
5.	2021-11-19T08:30:00-2021-11-20T02:30:00	27.9 (Enc.10)	202
6.	2022-02-25T12:30:00-2022-02-25T18:30:00	13.3 (Enc.11)	133
7.	2022-04-03T23:30:00-2022-04-09T07:30:00	156.9	79.5
8.	2022-05-30T17:30:00-2022-05-31T14:30:00	27.9	199.9
9.	2022-09-05T23:30:00-2022-09-06T05:30:00	13.3 (Enc. 13)	150.5
10.	2022-10-19T12:30:00-2022-10-19T13:30:00	163.4	70.9
11.	2022-10-20T06:30:00-2022-10-23T17:30:00	163.4	73.1
12.	2022-12-09T17:30:00-2022-12-10T09:30:00	25.8 (Enc. 14)	184.9

Note. The bold-texted row indicates the identified radial alignment period.

into switchbacks due to velocity shear. The variation in radial speed has been previously invoked to explain deformations of the heliospheric current sheet (S. T. Suess and E. Hildner 1985) and it has been previously suggested that they can have an important role in regulating turbulence in the solar wind (D. A. Roberts et al. 1992).

Switchbacks evolve to release their magnetic tension and reach pressure equilibrium with their surrounding environment (M. Akhavan-Tafti et al. 2021). M. Akhavan-Tafti et al. (2022) revealed that rotational discontinuity (RD)-type switchbacks undergo a relaxation process with an exponential decay rate of $0.06 [\text{Rs}^{-1}]$. This process leads to the formation of magnetic discontinuities with smaller normals. The relaxation process is estimated to contribute to the transfer of up to 16% of the total reconnected magnetic energy into the surrounding plasma. Magnetohydrodynamic (MHD) simulations by A. Tenerani et al. (2021b) show that magnetic switchbacks become increasingly unstable and eventually decay as they propagate away from the Sun.

The purpose of this study is to determine the process through which switchback magnetic energy reduces with heliocentric distance. To address this, we carefully analyzed switchbacks observed from two different locations in the inner heliosphere and identified their evolution characteristics. We investigated the magnetic and plasma characteristics of isolated and adjacent switchback events observed during a PSP–Solo radial alignment. Since no PSP–Solo radial alignments with identical solar source regions could be identified, this study used observations during a radial alignment containing parcels originating from similar magnetic footprints and solar source regions (plasma composition). The manuscript is organized as follows: In Section 2, we briefly introduce the data used in this study and the event identification algorithm and criteria. In Section 3, we discuss the observations and evolution characteristics of identified isolated/adjacent switchback events. Finally, in Section 4, we conclude this study and discuss future work.

2. Preliminary Data Sources and Event Identification Algorithm

In this study, we utilize data from the PSP FIELDS instrument (S. D. Bale et al. 2016), which provides magnetic field measurements at up to 290 samples per second. Additionally, we incorporate data from the PSP Solar Wind Electrons Alphas and Protons instrument suite (J. C. Kasper

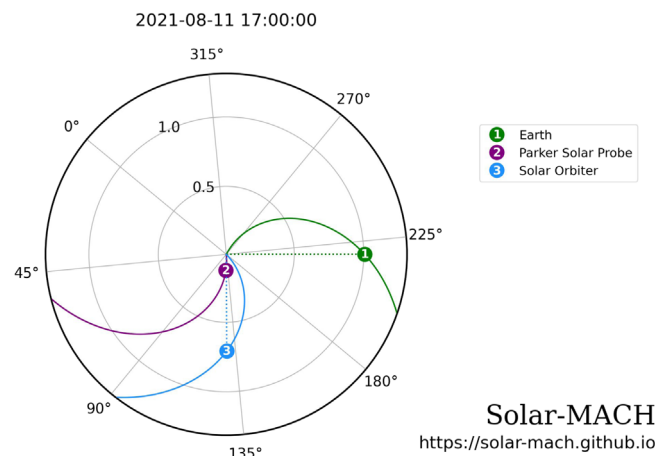


Figure 1. Position of PSP, Solo, and Earth on 2021 August 11 at 17:00:00 UT. The grid in black corresponds to the Stonyhurst coordinate systems. This polar plot is generated using the Solar-MACH tool (<https://serpentine-h2020.eu/tools/>; J. Gieseler et al. 2023).

et al. 2016), comprising the Solar Probe Cup and the Solar Probe Analyzers, providing solar wind parameters at up to 4 Hz cadence. Furthermore, we include data from the Solo MAG (T. S. Horbury et al. 2020) fluxgate magnetometer, offering 8 Hz magnetic field measurements, and Solo Solar Wind Analyzer (C. J. Owen et al. 2020), supplying electron (EAS sensor), proton, and alpha-particle (PAS sensor) 3D velocity distribution functions with up to 4 Hz resolution.

2.1. Radial Alignment Identification

The time intervals corresponding to the same plasma parcel observed at PSP and Solo during their radial alignment are determined using a ballistic approach. Following this method, as of the present date, we have identified 12 alignment durations for PSP and Solo. In our pursuit of pinpointing robust switchback events observed at various distances within the heliosphere, we meticulously applied three alignment selection criteria. The first criterion involves the spatial positioning of PSP in close proximity to the Sun (within $< 30 \text{ Rs}$), while Solo is positioned at a greater distance from the Sun ($> 130 \text{ Rs}$). The second criterion requires the period to contain the reversal of B_r , and the third criterion is contingent upon the availability of high-quality magnetic and plasma measurements from both the PSP and Solo spacecraft.

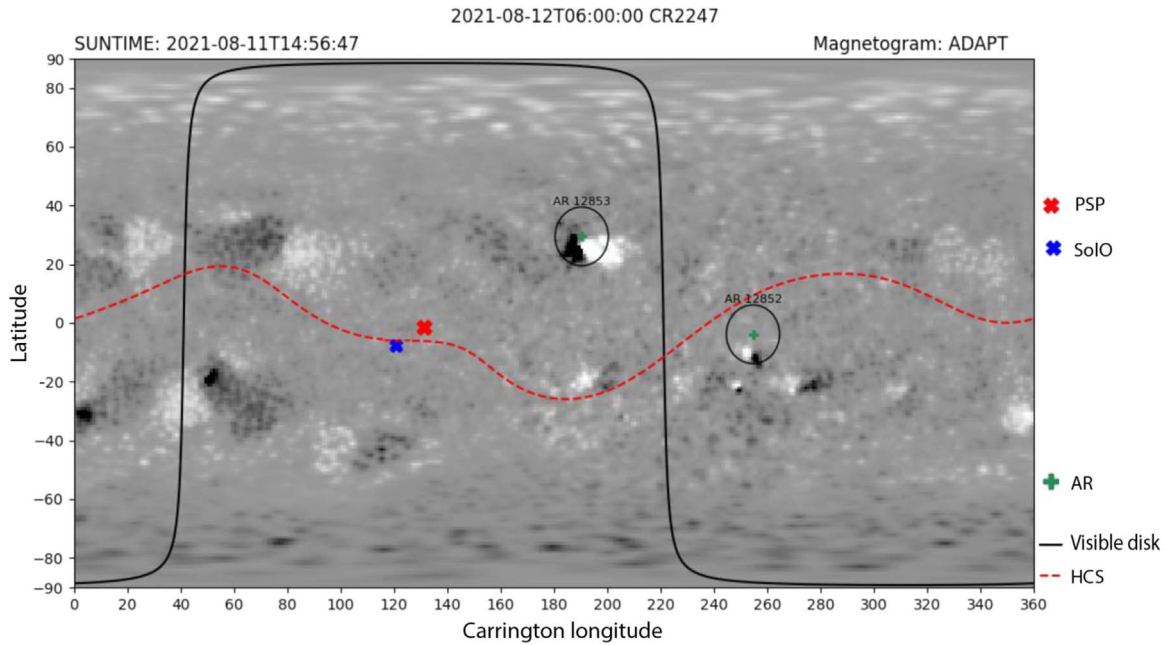


Figure 2. Instantaneous magnetic connectivity of PSP (red cross) and SoLo (blue cross) at the time considered, highlighting the subtle differences between both. The red dotted line presents the HCS.

Table 1 presents all 12 identified alignment durations with the corresponding distances of PSP and SoLo from the Sun. By considering the first and second criteria, we narrowed down our selection to 7 out of the initially reported 12 alignment durations. Subsequently, employing the third criterion, we identified only one alignment duration among the seven. The alignment duration #3 (from 2021-08-11T08:30:00 to 2021-08-12T09:30:00), when PSP was positioned at 25.8 Rs during its ninth encounter (E9) and SoLo was situated at 152 Rs, satisfied all three alignment selection criteria.

Figure 1 illustrates the relative locations of the observing spacecraft in the heliosphere, and Table 2 details their specific positions within the heliosphere, with Earth’s location included for reference. During E9 of PSP, it maintains a significantly close proximity to the Sun, with a heliocentric distance of 25.8 solar radii, while SoLo is positioned at 152 solar radii. PSP’s position is characterized by a Carrington longitude of 130° and a latitude of -1.4° , whereas SoLo occupies a slightly different position with a Carrington longitude of 126.4° and a latitude of -1.8° . Additionally, both spacecraft are situated behind Earth in terms of longitudinal separation, with PSP at -85.9° and SoLo at -89.5° . Similarly, their latitudinal separation from Earth is noteworthy, with PSP at -7.9° and SoLo at -8.3° . The magnetic footpoint Carrington longitudes of 118° for PSP and 136° for SoLo underscore their distinctive magnetic connections to the solar surface. These differences in location and distance, combined with their longitudinal and latitudinal separations, contribute to each spacecraft’s unique vantage point for studying the evolutionary phenomena of switchbacks.

The Magnetic Connectivity Tool (A.P. Rouillard et al. 2020, N Poirier et al. 2021) enables the estimation of the coronal origin of solar wind and energetic particles detected by various spacecraft. To achieve this, it simulates the coronal and interplanetary magnetic fields using a range of assumptions and methodologies. Presently, the magnetic field below the source surface (~ 2.5 solar radii), is calculated by a magnetic field extrapolation model, such as the potential field source

surface (PFSS) model (M. D. Altschuler and G. Newkirk, 1969, K. H. Schatten et al. 1969, M. Neugebauer et al. 2002), while the interplanetary magnetic field is presumed to follow a Parker spiral configuration. Recently, the footpoint of an in situ solar wind measurement can be established using a Magnetic connectivity tool,⁵ which uses the PFSS model and the boundary conditions of the magnetograms given by ADAPT/GONG and the radial field on the source surface, with an assumption that the solar wind speed is constant above the source surface. These maps clearly demonstrate that proximity to prominent topological features, such as large equatorial streamers and the heliospheric current sheet (HCS; red dotted line), can impact the estimations of connectivity and latitudinal separations.

Figure 2 shows the magnetic footprints of PSP (red cross) and SoLo (blue cross) on the Sun provided by the magnetic connectivity tool. This result shows the longitude separation between the footpoints of PSP and SoLo is less than 20° ; however, they are located at different sides of the HCS. The overall uncertainty in the position of the footpoint of the magnetic field lines as mapped by the PFSS model is within approximately 10° (M. Neugebauer et al. 2002, R. J. Leamon and S. W. McIntosh, 2009). Taking this $\sim 10^\circ$ of uncertainty into account, we think the difference between the PSP and SoLo footpoints is not substantial, or they can be considered similar within the range of the model’s uncertainty.

2.2. Identification of Robust Switchback

To identify prominent switchback candidates, the first criterion is to check the HCS crossing to ensure the magnetic field polarity. Then, to identify reversals in the radial component of the magnetic field (B_r) in the PSP and SoLo observations, we employed the well-established automated algorithm provided by M. Akhavan-Tafti et al. (2021) on the identified B_r -reversals with clear magnetic field signatures.

⁵ <http://connect-tool.irap.omp.eu/>

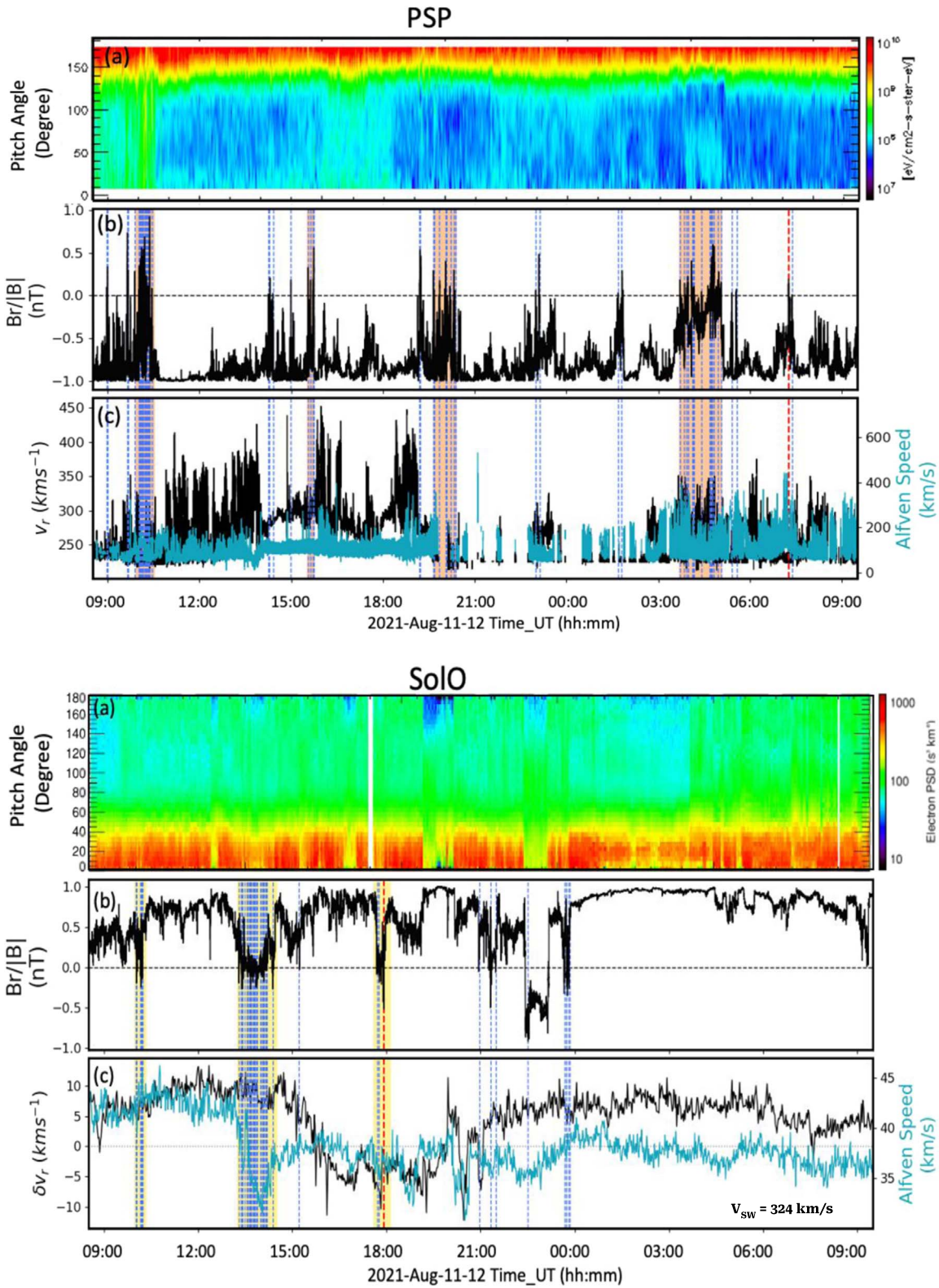


Figure 3. Shows the time interval from 2021 August 11 08:30:00 to 2021 August 12 09:30:00, when PSP and SoLo were radially aligned. In both PSP and SoLo, the top panels (a) show the normalized pitch angle distributions of suprathermal electrons (e-PADs) at an energy of 314 eV, middle panels (b) present the radial to total magnetic field ratio ($B_r/|B|$). Bottom panels (c) show the radial component of velocity along with local Alfvén speed. Dashed vertical blue lines indicate the number of magnetic field reversals during the spacecraft alignment period and the red dashed lines are for the reported events for PSP and SoLo. Orange shaded regions in PSP present the SBPs and yellow shaded regions in SoLo indicate the MSs.

These signatures are defined as having five distinct regions: the leading quiet solar wind (QL), the leading transition region (TL), the spike region with a steady magnetic field

(Spike), the trailing transition region (TT), and the trailing quiet solar wind (QT), along with radial velocity enhancement within the spike.

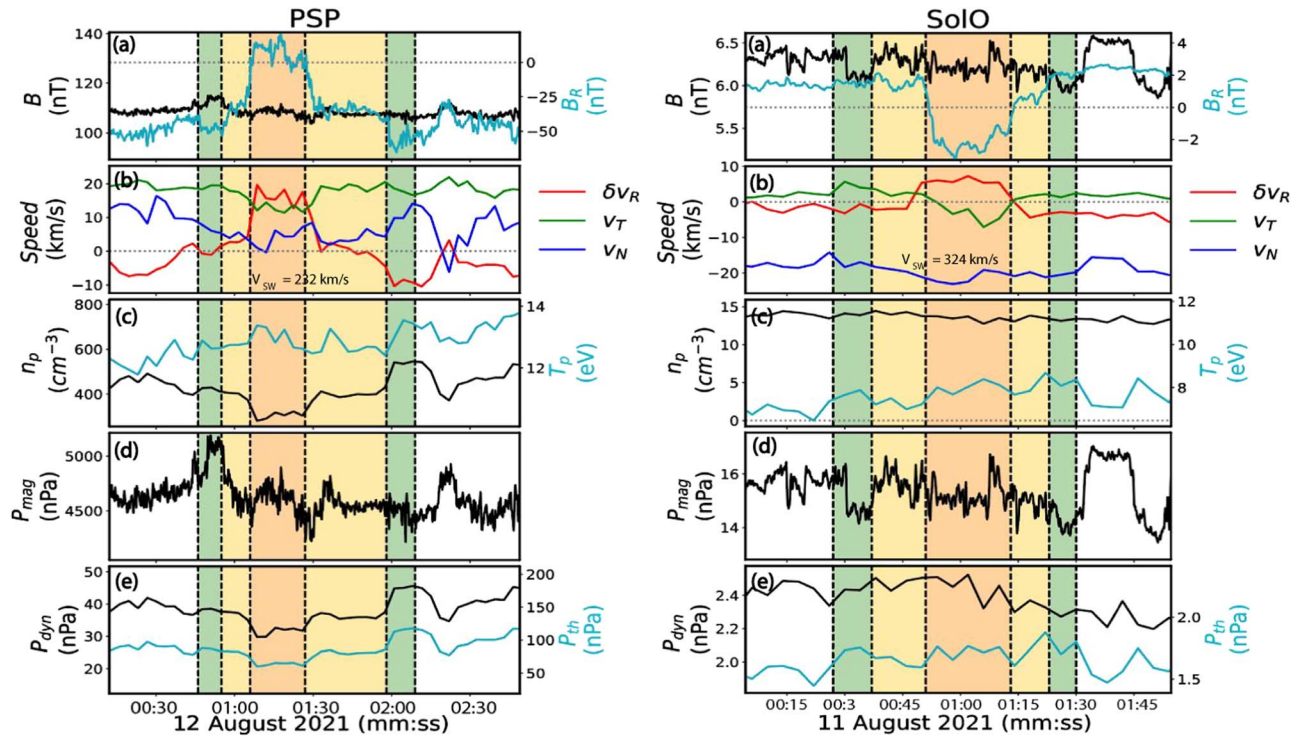


Figure 4. Left: PSP and right: SoLo. Panels top to bottom: (a) magnetic field ($|B|$, B_r), (b) velocity plasma moment (V_{rn}), (c) plasma density and temperature, (d) magnetic pressure, and (e) dynamic and thermal pressure. Green-shaded regions represent the QL and QT, respectively; yellow-shaded regions represent the TL and TT; and orange-shaded regions represent the spike.

During the alignment, PSP identified a substantial negative radial magnetic field (B_r) component with large variations changing to positive polarity, while SoLo observed the radial component of the magnetic field changing from positive to negative polarity. The solar wind radial velocity (V_r) also exhibited significant fluctuations. In Figure 3, the upper panels ((a) PSP and SoLo) display the pitch angle distribution (PAD) of suprathermal electrons. This population includes the “strahl” electrons that carry heat flux away from the Sun, always directed antisunward along open heliospheric field lines (W. Feldman et al. 1975). These electrons provide information about the polarity of the magnetic field lines at the source, even if, locally, the field lines may be bent or even reversed (M. J. Owens et al. 2017). The ratio of the radial magnetic field component (B_r) to the total magnetic field strength ($|B|$), i.e., $B_r/|B|$, is shown in the middle panels. The radial component of velocity and local Alfvén speed are plotted in panel (c). In the bottom panels ((b) and (c)), dashed blue lines indicate where $B_r/|B|$ changes polarity, but the dominating electron-PADs remain the same, representing a complete magnetic field reversal that typically characterizes the spike. We identified a total of 52 magnetic field reversals in PSP and 34 in SoLo during the third alignment duration.

To identify prominent and isolated reversals, we require the ratio of the radial magnetic field component ($|B_r|/|B|$) to shift significantly from the quiet solar wind to the spike. Specifically, we set criteria for the magnitude of the magnetic field reversal, such that $|B_r|/|B|$ should be >0.25 within the spike and <0.85 in the quiet period. Additionally, we look for an enhancement in velocity relative to spikes. In the case of a switchback, the radial velocity (V_r) should be greater than 2 times the local Alfvén speed at close proximity to the Sun and greater than the local Alfvén speed at further distances.

Applying the above criteria, we identified one switchback candidate at each spacecraft, indicated by red dashed lines in Figure 3 (panels (b) and (c) for both PSP and SoLo).

2.3. Identification of Switchback Patches and Microstreams

During a unipolar PAD period, a switchback patch (SBP) can be defined by the following criteria: (1) a duration of minutes to hours, (2) adjacent B_r reversals, (3) constant $|B|$, and (4) velocity enhancement within the spike regions (approximately twice to the local Alfvénic velocity). On the other hand, MSs are characterized by (1) duration of minutes to hours, (2) adjacent B_r reversals, (3) fluctuation in $|B|$, (4) moderate velocity enhancement ($20\text{--}30\text{ km s}^{-1}$ from the background), and (5) density enhancement (M. Neugebauer et al. 1995; M. Neugebauer and A. C. Sterling, 2021). In the reported alignment period, we observed four SBPs at PSP (orange-shaded regions in Figures 3(b) and (c)) and three MSs at SoLo (yellow-shaded regions in Figures 3(b) and (c)). It is important to note that SBPs are only observed near the Sun (at PSP), while MSs are solely observed farther away (at SoLo).

3. Results

3.1. Evolution of Switchbacks Observed at PSP and SoLo

In this section, we identified the observational signature of candidate switchbacks observed on 2021 August 12 at 07:00:00 UT at PSP and on 2021 August 11 at 17:55:00 UT at SoLo (Figure 4). In both plots, panels (a) and (b) display the magnetic field B with B_r and proton bulk velocity v in the RTN coordinates. To ease visualization, we subtracted the average proton bulk velocity $\langle v \rangle$ across the sampled interval from the data. The background solar wind speed was 232 km s^{-1} for the observed switchback at PSP, while it was 324 km s^{-1} for

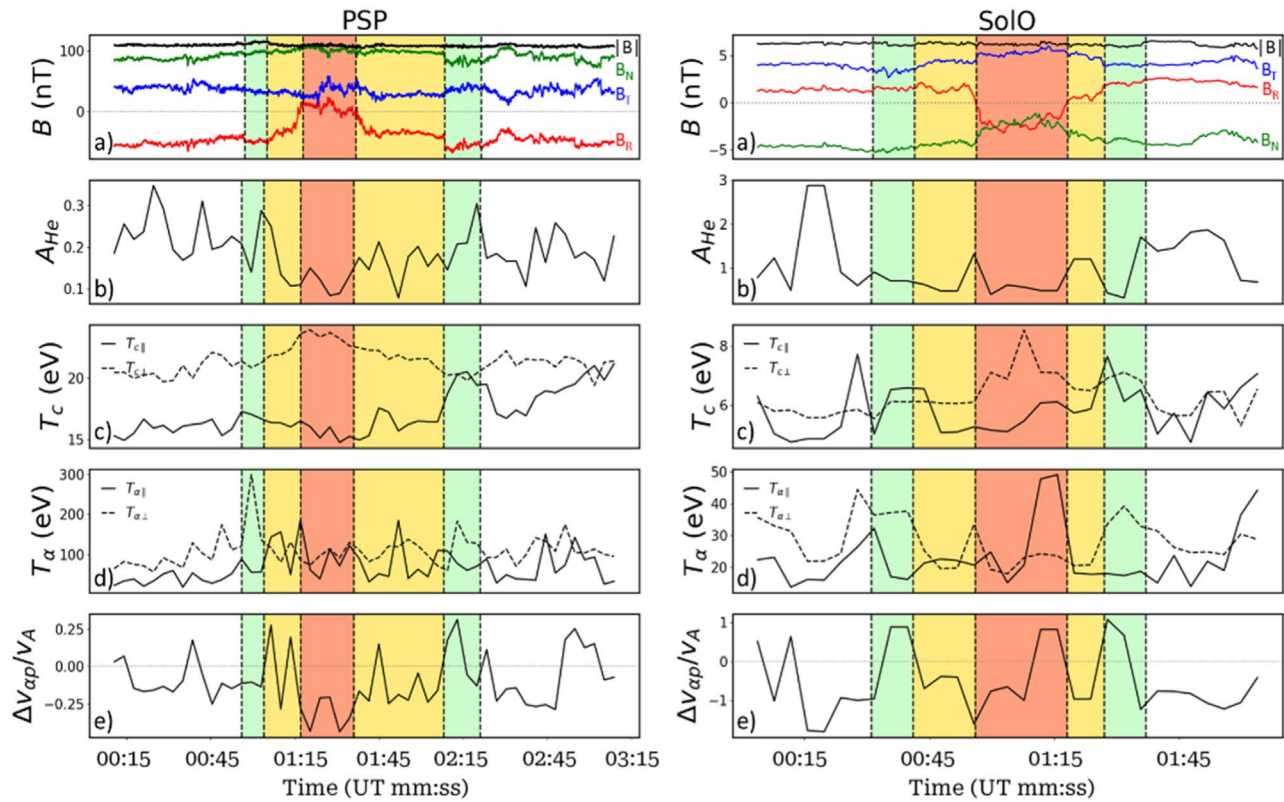


Figure 5. Left: PSP and right: SoLo. Panels top to bottom: (a) magnetic field ($|B|$, B_T , B_N), (b) He abundance, (c) proton core temperature (T_{perp} and T_{par}), (d) alpha temperature (T_{perp} and T_{par}), (e) alpha-proton differential speed. Green-shaded regions represent the QL and QT, respectively. Yellow-shaded regions represent the TL and TT, and orange-shaded regions represent the spike.

Table 2

Position of PSP, SoLo, and Earth on 2021 August 12 at 06:00:00 UT in the Inner Heliosphere

#	Earth	PSP	SoLo
Heliocent. distance (solar radii)	215	28.5	152
Carrington longitude (deg)	215.9	130	126.4
Carrington latitude (deg)	6.5	-1.4	-1.8
Longitude separation to Earth longitude (deg)	0	-85.9	-89.5
Latitude separation to Earth latitude (deg)	0	-7.9	-8.3
Magnetic footpoint Carrington longitude (deg)	278.7	118	136

the switchback observed at SoLo. Panel (c) shows the plasma density and temperature. Panel (d) presents the magnetic pressure (P_{mag}), and the bottom panel (e) displays the dynamic (P_{dyn}) and thermal (P_{th}) pressure.

PSP identified a substantial negative radial magnetic field (B_r) component with significant polarity changes, transitioning from negative to positive, while SoLo observed fluctuations shifting to negative polarity from positive. The solar wind radial velocity (V_r) is also highly variable and dominant compared to V_t and V_n . The variability in flow speed exhibited in switchbacks is directly related to the magnetic field (N. Raouafi et al. 2023). In the reported event, the jump in velocity is higher (7.26%) compared to SoLo (1.37%). In PSP's switchback, plasma density sharply decreases in the spike region, by approximately -25% (200 cm^{-3} magnitude), compared to the quiet solar wind. In the SoLo switchback, a slight decrease (-2.96%) is observed in spikes compared to the leading quiet and transition regions. While plasma temperature

Table 3

Estimated Jump (QL to Spike) of Magnetic Field and Plasma Parameters for Candidate Switchbacks

Jump (QL to Spike)	PSP (25.8 Rs)	SoLo (152 Rs)
Duration of Switchbacks (s)	85	72
$ B $ ($1/r^2$) (nT)	-4.06%	0.48%
Density ($1/r^2$) (cm^{-3})	-25.14%	-2.96%
Temp ($1/r^{\gamma-1}$) (eV)	1.03%	7.35%
$ V $ (km s^{-1})	7.26%	1.37%
P_{Mag} ($B^2/2\mu_0$) (nPa)	-0.82%	0.63%
P_{Dyn} (mpNpVp^2) (nPa)	-19.79%	-2.84%
P_{Th} ($N \text{ p KT p}$) (nPa)	-25.3%	5.76%

in both PSP and SoLo does not show any significant variation in different regions of switchbacks. The analysis shows that P_{mag} is relatively unchanged in PSP and SoLo observations. In contrast, P_{dyn} and P_{th} decrease at the switchback boundaries by up to -20% at PSP, while they remain relatively unchanged at SoLo (estimated values are presented in Table 3).

In solar wind, the alpha-proton signature is largely governed by conditions at the source region and thus provides useful information about its properties and the release mechanisms involved in the formation of the solar wind (M. R. Aellig et al. 2001; P. Bochsler, 2007; J. C. Kasper et al. 2012a, 2012b; C. Y.-Y. Huang et al. 2016; H. Fu et al. 2018; Z. Huang et al. 2023). Figure 5 shows the time series of various proton and alpha population parameters measured in the reported switchbacks. Panel (a) shows the magnetic field B and panel (b) shows

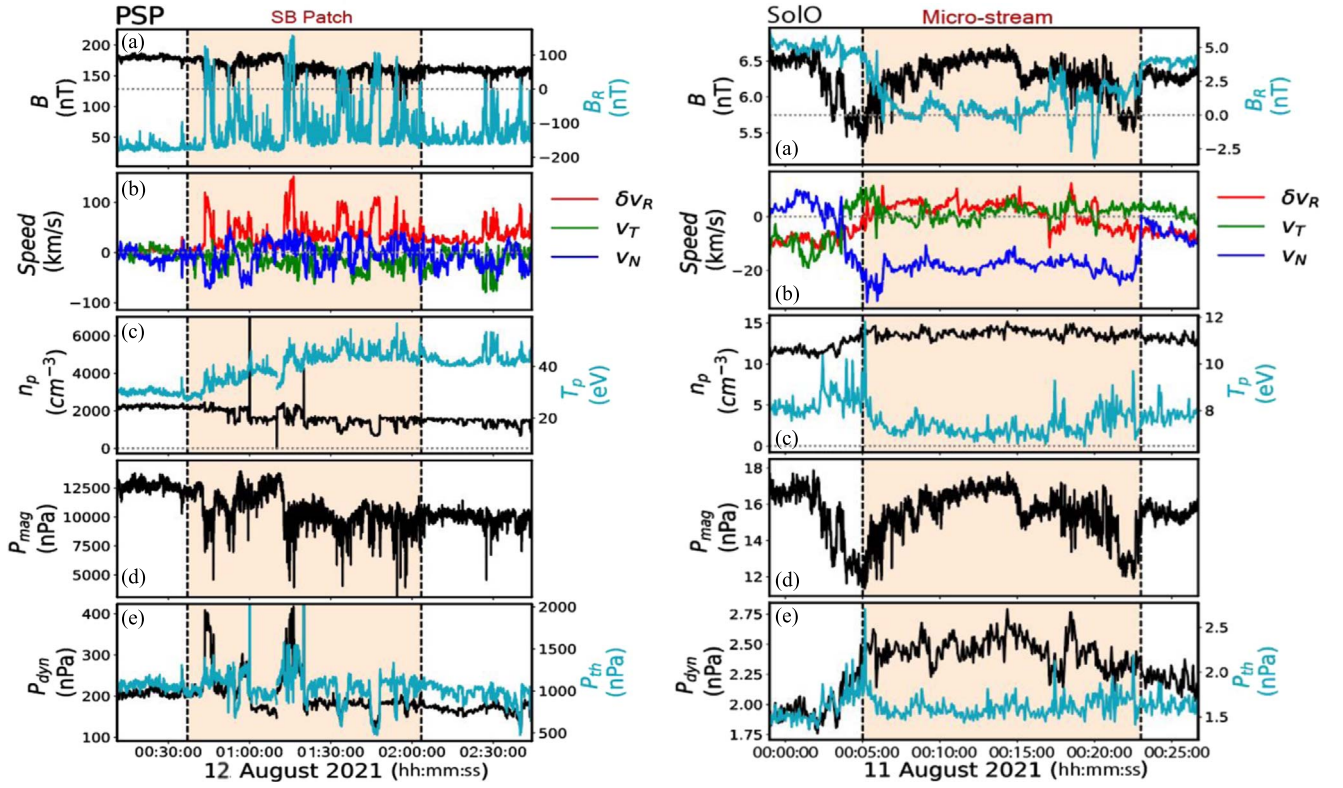


Figure 6. PSP (left) and SoLo (right): panels top to bottom: (a) magnetic field ($|B|$, B_r), (b) velocity plasma moment (V_{rm}), (c) proton density and temperature, (d) magnetic pressure, (e) dynamic and thermal pressure. The orange-shaded region is the SBP at PSP and MS at SoLo.

the helium abundance ratio $A_{\text{He}} = (n_{\alpha}/n_p) \cdot 100\%$, where n_{α} and n_p are the alpha and proton number density, respectively. Panels (c) and (d) show the parallel (T_{\parallel} , solid line) and perpendicular (T_{\perp} , dotted line) temperatures of the proton core T_c and alphas T_{α} , respectively. Panel (e) shows the signed magnitude of the alpha-proton velocity difference vector, $\Delta v_{\text{cp}} = |v_{\alpha} - v_p| \cdot \text{sgn}(v_{\alpha,R} - v_{p,R})$, normalized to the local Alfvén speed v_A (D. B. Reisenfeld et al. 2001; T. Durovcova et al. 2017; A. Fedorov et al. 2021). For the SoLo event, we obtained this data using the methods developed by R. De Marco et al. (2023).

Both of the observed switchbacks are embedded within slow solar wind streams containing helium-poor ($A_{\text{He}} \leq 1\%$) plasma. Inside the spike region of both events, A_{He} decreases slightly compared to its value in the surrounding solar wind. At PSP, A_{He} decreases from $\sim 0.2\%$ in the TL and TT regions to 0.1% inside the spike region. A_{He} in the TL and TT regions does not change compared to the QL, QT, and switchback exterior regions. In the case of the SoLo switchback, A_{He} is higher before and during the switchback encounter compared to after the encounter and is overall smaller compared to PSP. A_{He} decreases to 1% compared to the QT region. It indicates that reported switchbacks observed within slow solar wind having decreased A_{He} (helium-poor population) should be threaded to helmet streamer regions (J. C. Kasper et al. 2007, 2012; B. L. Alterman et al. 2018; B. L. Alterman and J. C. Kasper, 2019).

In slow solar wind, the parallel temperature of proton/alpha should be higher than the parallel proton/alpha temperature (Q. H. Li et al. 2023). However, there is no significant variation in either component that can be attributed to the switchbacks. Δv_{cp} increases toward the Sun but the magnitude is mainly below v_A , and alpha particles usually move faster than protons

near the Sun, based on PSP observations. However, the high $\Delta v_{\text{cp}}/v_A$ in the solar wind may be associated with the very low local Alfvén speed when magnetic field lines change polarity, or it may point to the preferential acceleration of alpha particles (P. A. Isenberg and J. V. Hollweg, 1983; J. C. Kasper et al. 2017). The average $\Delta v_{\text{cp}}/v_A$ is observed between -0.15 and -0.2 outside the spike region although there are large fluctuations, particularly in the TL and QT regions. Inside the spike region, we observe a minimum average $\Delta v_{\text{cp}}/v_A$ of ~ -0.4 . The negative values of $\Delta v_{\text{cp}}/v_A$ could be a result of waves that slow down alpha particles but accelerate the protons as the energy of alpha particles exceeds that of protons (T. Durovcova et al. 2017).

3.2. Evolution of Switchback Bundles Observed at PSP and SoLo

Within this radial alignment, we observed four SBPs with PSP and three MSs with SoLo. Notably, no MSs were observed by PSP, and no switchbacks were detected by SoLo. Figure 6 shows an example of an SBP observed at PSP and an MS observed at SoLo, where the top panel shows the radial component of the magnetic field B_r to the magnitude B averaged followed by velocity components, density temperature, magnetic, thermal, and dynamic pressure. At PSP the shaded region indicates the SBP for the duration of 80 minutes with constant B_r reversals associated with velocity jump along with constant total magnetic field. However, at SoLo, the shaded region depicts the boundaries of an MS for a duration of ~ 20 minutes with a slight enhancement in velocity and density. Notably, in the MS, only six B_r reversals were found.

By analyzing all identified SBPs at PSP and MSs at SoLo, we observed that the MSs contain a 30% lesser number of

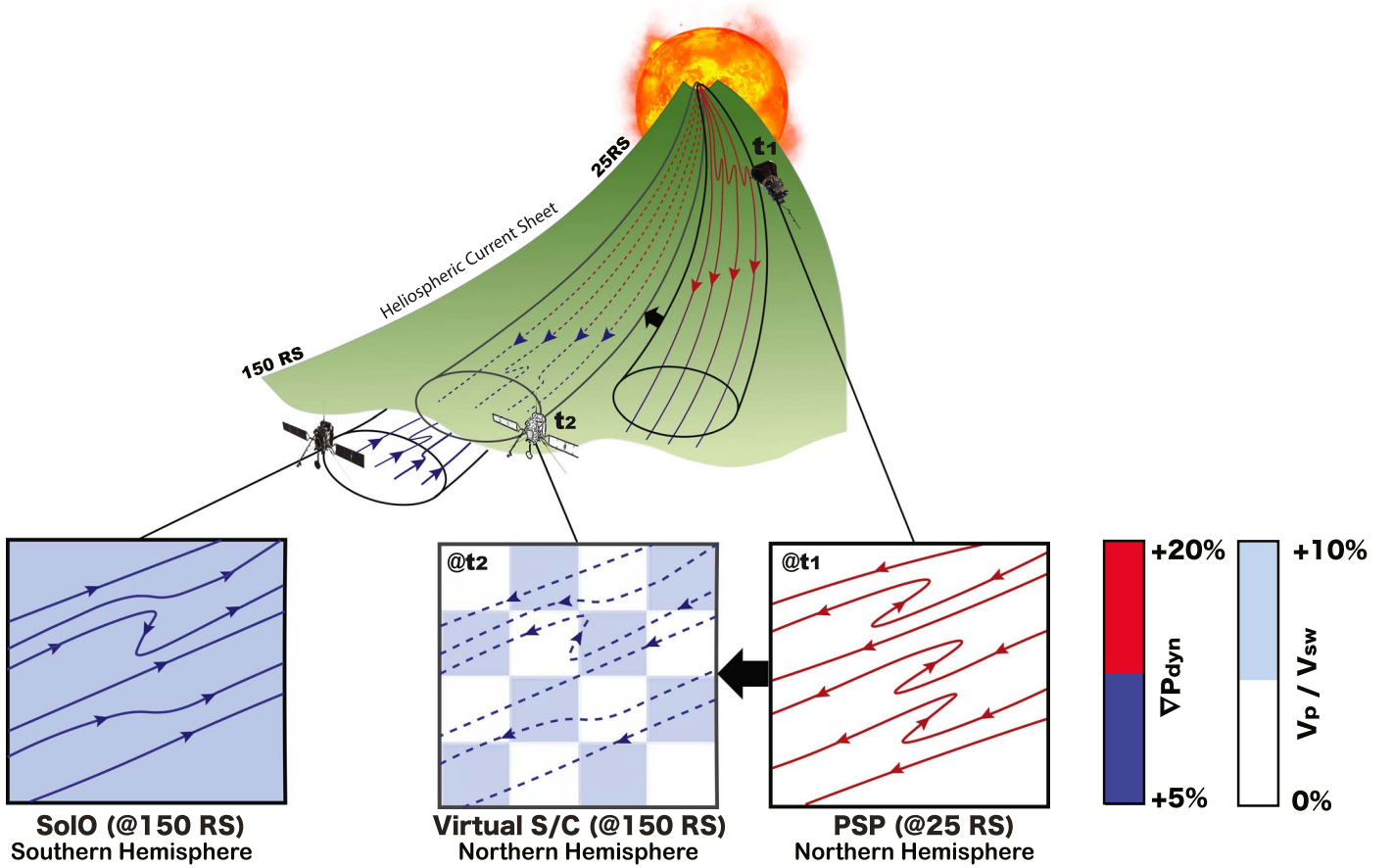


Figure 7. Concept illustration of the spatial and temporal evolution of a magnetic switchback. The color bars indicate dynamic pressure (P_{dyn}) and relative velocity (V_p/V_{sw}). The boxes with solid lines represent actual observations, while those with dotted lines depict hypothetical observations if viewed from the same side of the heliospheric current sheet (HCS). The green layer represents the HCS, arrows indicate the magnetic field direction, and the checkered background at the virtual spacecraft location highlights the observational uncertainty in this hypothetical scenario.

switchbacks to the SBPs. Additionally, we found that, in MSs, the background proton velocity (v_p) is approximately 10% higher than the pristine solar wind, while in SBPs, v_p is comparable to the solar wind velocity (v_{sw}). This underscores that the MSs could potentially emerge as a product of continuous and lasting increases in velocity that stem from a sequence of switchbacks.

4. Discussion and Conclusion

This investigation aims to compare switchback properties at two different heliocentric distances during a radial alignment of PSP and SoLO, with the goal of studying the evolution characteristics of switchbacks. Since no identical parcel of magnetic field and plasma was identified to pass over both spacecraft at different distances, this study analyzes switchbacks inside two parcels that originated from similar magnetic footprints and plasma source regions during a PSP–SoLO radial alignment.

The key results, based on the observed magnetic and plasma characteristics of switchbacks observed at PSP and SoLO, are as follows:

1. This study examines switchbacks within two distinct plasma parcels observed at distinct locations in the inner heliosphere. To justify their comparison, initially, their magnetic footprints using ballistic mapping were analyzed, revealing a proximity of only $\sim 20^\circ$, highlighting magnetic

connectivity to a similar solar source region. Further confirmation through analysis of plasma and compositional data indicates a similar generation mechanism and source regions for both parcels. This comparison is valid as it underscores the consistency and coherence between the magnetic footprints and the compositional characteristics, reinforcing the notion of shared origins and behaviors within the heliospheric environment.

- a. In the slow solar wind, switchback events rooted from similar magnetic footprints are observed with helium-poor plasma ($A_{\text{He}} < 1\%$) and low $\Delta v_{\alpha p}/v_A$ population, indicating that switchbacks may have originated from a similar source region (helmet or streamer-like structures; Durovcova et al. 2017, 2019; H. Fu et al. 2018; Section 3.1).
2. Magnetic and plasma observations at the switchback leading transition regions show that P_{mag} is relatively unchanged in both PSP and SoLO observations. In contrast, P_{dyn} and P_{th} sharply drop across the switchback boundary at PSP by up to $\sim -20\%$, while they remain relatively unchanged at SoLO (Section 3.1).
 - a. The magnetic and plasma observations at the switchback boundary regions at PSP and SoLO indicate that the switchback plasma population may come to equilibrium with the surrounding environment with heliocentric distance. The equilibrium further points to a possible flow of plasma and energy across switchback

boundaries with heliocentric distance, in agreement with M. Akhavan-Tafti et al. (2022) who argued that switchbacks are dominantly permeable, rotational-type magnetic discontinuities.

- b. The RD-type boundaries near the Sun likely influence the dynamics of the switchbacks (M. Akhavan-Tafti et al. 2022), enabling the efficient exchange of material and energy that, in turn, contributes to the overall stability and equilibrium observed across varying distances within the heliosphere.
3. Observation shows that bundles of switchbacks are observed as SBPs at PSP and solely observed as MSs at SoLO. Observed MSs contain 30% fewer switchbacks than SBPs. Furthermore, notable variations emerge in the background proton velocity (v_p) within these phenomena. In MSs, the background proton velocity (v_p) is approximately 10% greater than the pristine solar wind, while in SBPs, v_p is approximately equal to the solar wind velocity (v_{sw}). Additionally, the switchback dynamic pressure jump is greater in SBPs than in MSs (Section 3.2).
 - a. The smaller number of switchbacks observed in MSs suggests that some of the switchbacks inside the SBPs may dissipate with distance.
 - b. The dissipation of switchbacks can result in accelerating background plasma. The velocity enhancement inside of MSs may be a consequence of a relaxation of adjacent switchbacks with heliocentric distance.
 - c. In this scenario, it is conceivable that the switchback population equilibrates with the surrounding environment as it moves further in the heliosphere by dissipating its magnetic energy to background plasma. This, in turn, can result in SBPs evolving into microstreamers over time and heliocentric distance.

4.1. Interpretation

Figure 7 shows a cartoon illustration of our proposed mechanism—SBPs evolving into MSs over time and heliocentric distance. The evolution involves switchbacks within SBPs straightening, and therefore, depositing their excess magnetic energy into background plasma. Notably, the figure highlights the fact that the observed plasma parcels during the PSP and SoLO radial alignment were sampled from opposite hemispheric sides of HCS, thus radially inward versus outward magnetic field lines. It is plausible that a virtual spacecraft on the same hemispheric side of HCS as PSP, though farther out in heliocentric distance (@150 RS), would have observed the same flux tube with the same field polarity, except with dissipated switchbacks, shown as dashed field lines. Whether the background plasma in the flux tube would have had similar characteristics as that observed at SoLO is unknown.

The proposed mechanism is based on our observation that SBPs are found to occur more frequently in proximity to the Sun, while MSs are more commonly observed at greater distances. Furthermore, our observations indicated a difference in the dynamic pressure jump associated with switchbacks in patches versus MSs. The dynamic pressure jump is found to be greater (approximately 20%) in the switchback population.

We also observed that SBPs have a relatively higher concentration of switchbacks compared to MSs. Therefore, it









is hypothesized that magnetic relaxation may be responsible for converting the excess SBP magnetic energy into particle kinetic energy. This relaxation can also explain the observed velocity enhancement in the MSs observed at SoLO, possibly stemming from the relaxation of a series of switchbacks within SBPs and accelerating plasmas within MSs over time.

In summary, the combined measurements from PSP and SoLO significantly advance our understanding of how switchbacks evolve throughout their propagation, unveiling the remarkable endurance of these transients. Future work will focus on the statistical analysis of switchbacks identified at various distances in the heliosphere to validate their origins, formation, and evolution. Source region mapping will be crucial for understanding “in situ” and/or “ex situ” generation mechanisms of switchbacks. Additionally, it will offer valuable insights into the magnetic and plasma interactions that shape the inner heliosphere, while also shedding light on their role in solar wind heating.

Acknowledgments

The data used in this paper can be downloaded from <https://pdf.gsfc.nasa.gov/>. The authors are grateful for the dedicated efforts of the PSP and SoLO team. This work was supported by NASA contract Nos. NNN06AA01C, 80NSSC20K1847, 80NSSC20K1014, and 80NSSC21K1662. Solar Orbiter is a space mission run as an international collaboration between ESA and NASA and operated by ESA. Solar Orbiter SWA data were derived from scientific sensors that were designed and created and are operated under funding provided by numerous contracts from UKSA, STFC, the Italian Space Agency, CNES, the French National Centre for Scientific Research, the Czech contribution to the ESA PRODEX program and NASA. SO SWA work at the UCL/Mullard Space Science Laboratory is currently funded by STFC (grant Nos. ST/W001004/1 and ST/X/002152/1). L.Z. acknowledges support from NASA grants 80NSSC21K0579 and 80NSSC22K1015, NSF SHINE grant 2229138, and NSF Early Career grant 2237435.

ORCID iDs

Shirsh Lata Soni  <https://orcid.org/0000-0002-5550-739X>
 Mojtaba Akhavan-Tafti  <https://orcid.org/0000-0003-3721-2114>
 Gabriel Ho Hin Suen  <https://orcid.org/0000-0002-9387-5847>
 Justin Kasper  <https://orcid.org/0000-0002-7077-930X>
 Marco Velli  <https://orcid.org/0000-0002-2381-3106>
 Rossana De Marco  <https://orcid.org/0000-0002-7426-7379>
 Liang Zhao  <https://orcid.org/0000-0002-5975-7476>
 Christopher J Owen  <https://orcid.org/0000-0002-5982-4667>

References

- Aellig, M. R., Lazarus, A. J., & Steinberg, J. T. 2001, *GeoRL*, 28, 2767
 Akhavan-Tafti, M., Kasper, J., Huang, J., & Bale, S. 2021, *A&A*, 650, A4
 Akhavan-Tafti, M., Kasper, J., Huang, J., & Thomas, L. 2022, *ApJL*, 937, L39
 Akhavan-Tafti, M., & Soni, S. L. 2024, *ApJL*, 970, L26
 Alterman, B. L., & Kasper, J. C. 2019, *ApJL*, 879, L6
 Alterman, B. L., Kasper, J. C., Stevens, M. L., & Koval, A. 2018, *ApJ*, 864, 112
 Altschuler, M. D., & Newkirk, G. 1969, *SoPh*, 9, 131
 Bale, S. D., Badman, S. T., Bonnell, J. W., et al. 2019, *Natur*, 576, 237
 Bale, S. D., Goetz, K., Harvey, P. R., et al. 2016, *SSRv*, 204, 49
 Bochsler, P. 2007, *A&ARv*, 14, 1
 De Marco, R., Bruno, R., Jagarlamudi, V. K., et al. 2023, *A&A*, 669, A108
 Drake, J. F., Agapitov, O., Swisdak, M., et al. 2021, *A&A*, 650, A2

- Durovcova, T., Nemecek, Z., & Safrankova, J. 2019, *ApJ*, 873, 24
- Durovcova, T., Safrankova, J., Nemecek, Z., & Richardson, J. D. 2017, *ApJ*, 850, 164
- Fedorov, A., Louarn, P., Owen, C. J., et al. 2021, *A&A*, 656, A40
- Feldman, W., Asbridge, J., Bame, S., Montgomery, M., & Gary, S. 1975, *JGR*, 80, 4181
- Fu, H., Madjarska, M. S., Li, B., Xia, L., & Huang, Z. 2018, *MNRAS*, 478, 1884
- Gieseler, J., Dresing, N., Palmroos, C., et al. 2023, *FrASS*, 9, 384
- Horbury, T. S., O'Brien, H., Carrasco Blazquez, I., et al. 2020, *A&A*, 642, A9
- Huang, C. Y.-Y., Huang, Y., Su, Y.-J., et al. 2016, *JSWSC*, 6, A4
- Huang, Z., Sioulas, N., Shi, C., et al. 2023, *ApJL*, 950, L8280
- Isenberg, P. A., & Hollweg, J. V. 1983, *JGR*, 88, 3923
- Kahler, S. W., Crooker, N. U., & Gosling, J. T. 1996, *JGR*, 101, 24373
- Kasper, J., Stevens, M., Korreck, K., et al. 2012a, *ApJ*, 745, 162
- Kasper, J. C., Abiad, R., Austin, G., et al. 2016, *SSRv*, 204, 131
- Kasper, J. C., Bale, S. D., Belcher, J. W., et al. 2019, *Natur*, 576, 228
- Kasper, J. C., Klein, K. G., Weber, T., et al. 2017, *ApJ*, 849, 126
- Kasper, J. C., Stevens, M. L., Korreck, K. E., et al. 2012b, *ApJ*, 745, 162
- Kasper, J. C., Stevens, M. L., Lazarus, A. J., Steinberg, J. T., & Ogilvie, K. W. 2007, *ApJ*, 660, 901
- Landi, S., Hellinger, P., & Velli, M. 2006, *GeoRL*, 33, L14101
- Leamon, R. J., & McIntosh, S. W. 2009, *ApJ*, 697, L28, IOP
- Li, Q. H., Xiang, L., Wu, D. J., et al. 2023, *A&A*, 676, A137
- Mallet, A., Squire, J., Chandran, B. D., Bowen, T., & Bale, S. D. 2021, *ApJ*, 918, 62
- Montagud-Camps, V., Grappin, R., & Verdini, A. 2018, *ApJ*, 853, 153
- Mozer, F. S., Agapitov, O. V., Bale, S. D., et al. 2020, *ApJS*, 246, 68
- Neugebauer, M., Goldstein, B. E., McComas, D. J., Suess, S. T., & Balogh, A. 1995, *JGR*, 100, 23389
- Neugebauer, M., Liewer, P. C., Smith, E. J., Skoug, R. M., & Zurbuchen, T. H. 2002, *JGRA*, 107, 1488
- Neugebauer, M., & Sterling, A. C. 2021, *ApJL*, 920, L31
- Owen, C. J., Bruno, R., Livi, S., et al. 2020, *A&A*, 642, A16
- Owens, M. J., Lockwood, M., & Riley, P. 2017, *NatSR*, 7, 41548
- Poirier, N., Rouillard, A. P., Kouloumvakos, A., et al. 2021, *FrASS*, 8, 84
- Raouafi, N., Matteini, L., Squire, J., et al. 2023, *ApJ*, 945, 28
- Reisenfeld, D. B., Gary, S. P., Gosling, J. T., et al. 2001, *JGR*, 106, 5693
- Roberts, D. A., Goldstein, M. L., Matthaeus, W. H., & Ghosh, S. 1992, *JGR*, 97, 17,115
- Rouillard, A. P., Pinto, R. F., Vourlidas, A., et al. 2020, *A&A*, 642, A2
- Ruffolo, D., Matthaeus, W. H., Chhiber, R., et al. 2020, *ApJ*, 902, 94
- Schatten, K. H., Wilcox, J. M., & Ness, N. F. 1969, *SoPh*, 6, 442
- Schwadron, N. A., & McComas, D. J. 2021, *ApJ*, 909, 95
- Squire, J., Chandran, B. D., & Meyrand, R. 2020, *ApJL*, 891, L2
- Suess, S. T., & Hildner, E. 1985, *JGR*, 90, 9461
- Tenerani, A., Sioulas, N., Matteini, L., et al. 2021a, *ApJL*, 919, L31
- Tenerani, A., Sioulas, N., Matteini, L., et al. 2021b, *ApJL*, 919, L31
- Tenerani, A., & Velli, M. 2018, *ApJL*, 867, L26
- van Ballegooijen, A. A., Asgari-Targhi, M., Cranmer, S. R., & DeLuca, E. E. 2011, *ApJ*, 736, 3
- Zank, G. P., Nakanotani, M., Zhao, L.-L., Adhikari, L., & Kasper, J. 2020, *ApJ*, 903, 1